DOI 10.1007/s11094-024-03190-2
Pharmaceutical Chemistry Journal, Vol. 58, No. 4, July, 2024 (Russian Original Vol. 58, No. 4, April, 2024)

RADIOCOMPLEXATION, QUALITY CONTROL AND BIOEVALUATION OF [^{99m}Tc]TRICARBONYL ROLIPRAM FOR BRAIN IMAGING IN MICE

M. H. Sanad,[1,*] H. M. Eyssa,[2] S. M. Abd-Elhaliem,[1,*] A. B. Farag,[3] and Sabry A. Bassem[4]

Original article submitted May 9, 2023.

In this work, the complex of [^{99m}Tc]tricarbonyl rolipram was labeled utilizing a [^{99m}Tc]tricarbonyl core. Many optimal parameters have been used such as substrate (100 μg), pH of the reaction mixture (pH 9), reaction time (30 min), as well as temperature (100°C), providing an optimal radiochemical purity of 97.0%. Biodistribution investigations of our radiotracer, [^{99m}Tc]tricarbonyl rolipram, were conducted on normal Swiss Albino mice. The results indicated maximum brain uptakes of 8.2 %ID/g tissue at 10 min post injection (p.i.), which cleared from the brain with time until it reached 1.90 ± 0.17% at 1 h p.i. Therefore, [^{99m}Tc]tricarbonyl rolipram complex may be an excessively bio-selective receptor-tracer for brain ulcer imaging through the phosphodiesterase-4 inhibitor.

Keywords: Rolipram; [^{99m}Tc]tricarbonyl core; brain imaging; molecular modeling; docking.

INTRODUCTION

Many techniques have been used in brain imaging, either by direct or indirect methods [1–10]. The fast development of nuclear medicine throughout the last 25 years was in mainly due to the success of brain tumor imaging using radiopharmaceuticals designed to identify changes in the blood–brain barrier. Brain imaging requires the selection of certain compounds with high binding affinity to selective receptors such as phosphodiesterase-4 inhibitor. Rolipram was discovered and developed as a potential antidepressant drug [11, 12]. The phosphodiesterases are a group of enzymes that degrade the phosphodiester bond of secondary messengers such as cyclic adenosine monophosphate (cAMP) and cyclic guanosine monophosphate and then terminate their own action [13–20]. Recently, there has been increasing interest in agents that can enter the brain and are designed to provide functional data ranging from regional perfusion and metabolism to the distribution of binding sites for neuroactive compounds. Rolipram is one of the selective phosphodiesterase (PDE)4 inhibitors [21–23]. PDE4 is mostly found in the nerve and immune cells, and is capable of hydrolyzing cAMP. Most increments of cAMP levels can inhibit pro-inflammatory processes such as chemotaxis, degradation, and phagocytosis. The aim of the current work was to evaluate the possible use of [^{99m}Tc]tricarbonyl rolipram for brain imaging and to study the bio-distribution of [^{99m}Tc]tricarbonyl rolipram in Swiss Albino mice.

EXPERIMENTAL

Rolipram was purchased from Sigma-Aldrich. Thin-layer chromatography (TLC) aluminum sheets (20 × 25 cm) SG-60 F_{254} were supplied by Merck. All chemicals were of analytical or clinical grade and were used directly without further purification unless otherwise stated. A well-type NaI scintillation γ-Counter model Scalar Ratemeter SR7 (Nuclear Enterprises Ltd., USA) was used for radioactive measurement, which is a perfect NaI scintillation counter. Paper electrophoresis (PE) apparatus from E.C. Corporation (Albany, OR, USA) was used. All chemicals, as well as solutions, were bought from Merck (Kenilworth, NJ, USA), with the exception of pantoprazole, which was ob-

[1] Labeled Compounds Department, Hot Laboratories Center, Egyptian Atomic Energy Authority, P. O. Box 13759, Cairo, Egypt.
[2] Radiation Chemistry Department, National Center for Radiation Research and Technology,.
[3] Egyptian Atomic Energy, Authority, Cairo, 13759 Egypt.
[4] Pharmaceutical Chemistry Department, Faculty of Pharmacy, Ahram Canadian University, Giza, Egypt.
[5] Food Toxicology and Contaminants Department, National Research Centre, Dokki, Cairo, PB12622, Egypt.
* e-mails: drsanad74@gmail.com; sayedabdelhalim488@gmail.com

0091-150X/24/5804-0652 © 2024 Springer Science+Business Media, LLC

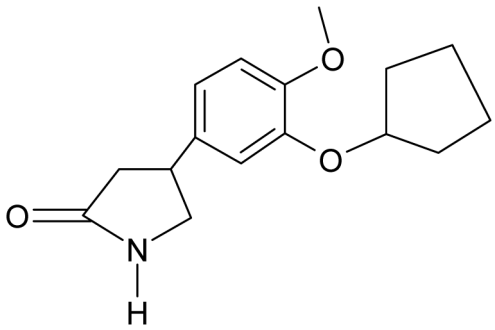

Fig. 1. The structure of rolipram.

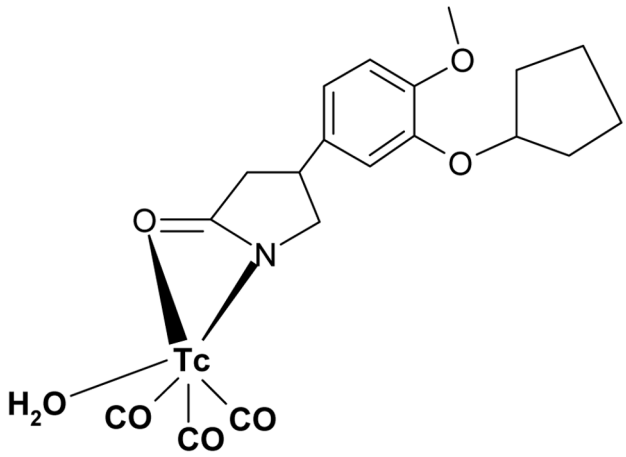

Fig. 2. The proposed structure of [^{99m}Tc]tricarbonyl rolipram.

tained from Sigma-Aldrich in the USA; pertechnetate [$^{99m}TcO_4^-$] was extracted from a $^{99}Mo/^{99m}Tc$ generator from Elutec (Brussels, Belgium). The National Research Centre donated *H. pylori* (Cairo, Egypt). Merck supplied the aluminum sheets used in thin-layer chromatography (TLC) (20 × 25 cm, SG-60 F254). High-performance liquid chromatography (HPLC) was performed using a Shimadzu LC-9A pump, a Rheodyne injector, an SPD-6A UV spectrophotometer sensor set at 254 nm, and a C-8, 250 × 4.6 mm, 5-µm, Lichrosorb reversed-phase column. At a 0.6-mL gradient flow rate per min, a sample of [^{99m}Tc]tricarbonyl rolipram in a volume of 10 µL was introduced onto a C-8 (Lichrosorb, 250 mm × 3 mm, 5 µm) column. Utilizing a fraction collector, 0.6-mL volumes were collected independently to reach a final volume of 25 mL, which was then recorded in a perfect NaI(Tl) counter (BLC-20, BUCK Scientific). Triethyl ammonium phosphate (solvent A) as well as methanol (the mobile phase) were each at a concentration of 0.05 M (solvent B). The gradient method was implemented in accordance with the published literature [24–31].

Radiolabeling

Radiosynthesis of [^{99m}Tc]-tricarbonyl precursor

Fac-[^{99m}Tc $(CO)_3(H_2O)_3$]$^+$, a [^{99m}Tc]tricarbonyl core, was prepared in accordance with Alberto, et al. [32]. An RP-HPLC and a Millipore filter with a pore size of 0.22 nm helped to calculate the radiosynthesis yield and core stability of [^{99m}Tc]tricarbonyl.

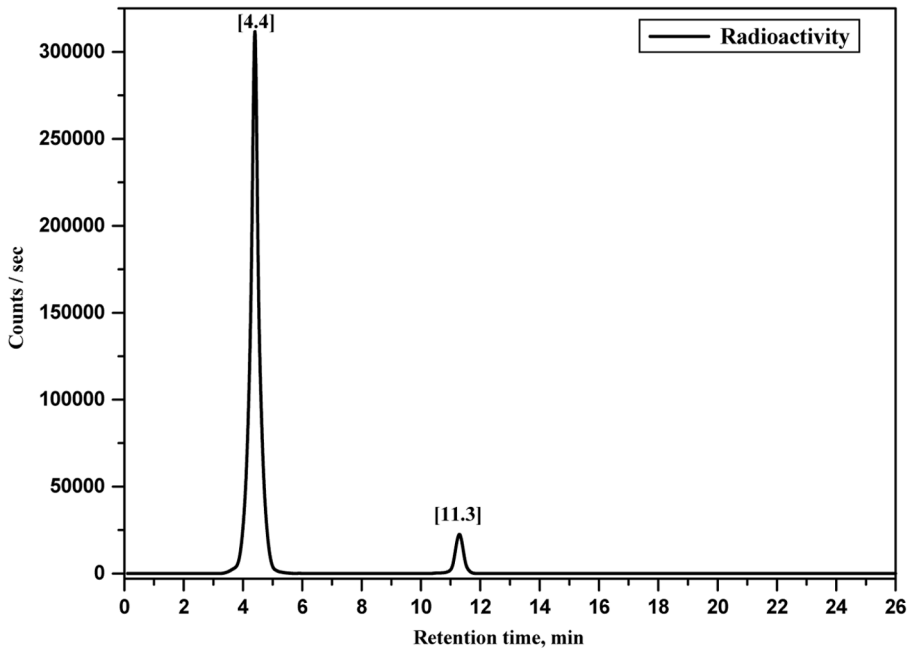

Fig. 3A. The HPLC radio-chromatogram of [^{99m}Tc]tricarbonyl precursor at R_t = 4.4 min and R_t = 11.30 min for free [^{99m}Tc]pertechnetate.

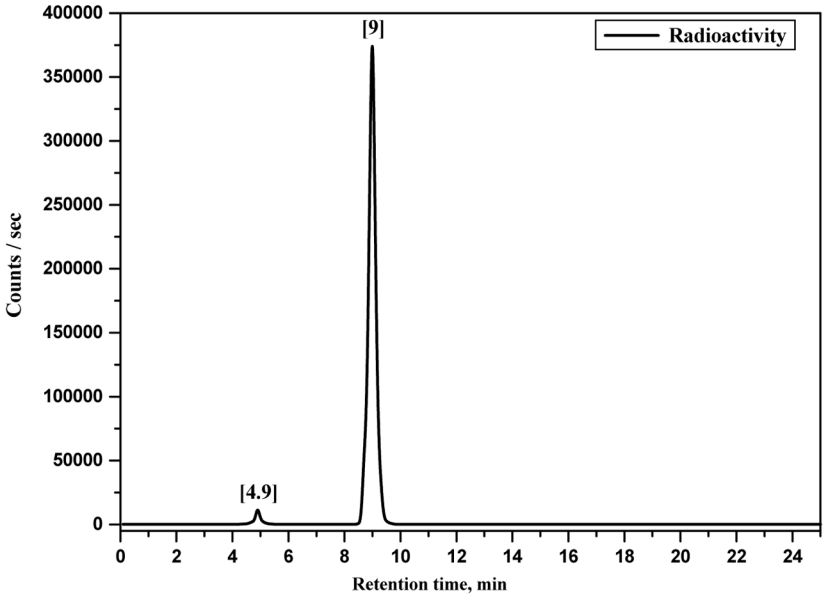

Fig. 3B. HPLC analysis. The R_t values of free [^{99m}Tc]tricarbonyl and [^{99m}Tc]tricarbonyl rolipram complex were 4.9 and 9 min respectively.

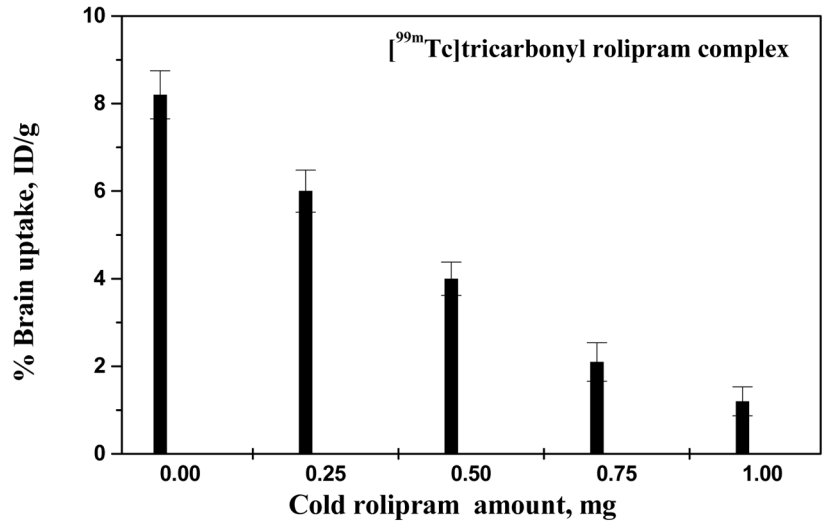

Fig. 4A. [^{99m}Tc]Tricarbonyl rolipram complex inhibition brain uptakes in normal male Swiss Albino mice at 10 min p.i. (% ID/g ± SEM, $n = 5$).

Radiolabeling procedure of [^{99m}Tc]tricarbonyl rolipram

The volume of the reaction mixture was held constant at around 2000 µL. At room temperature, 1 mL of the [^{99m}Tc]tricarbonyl core was combined with 100 µg pantoprazole diluted in ethanol (1 mg: 1 mL), accompanied by 100 µL of pH 9.0. (potassium phosphate buffer). Moreover, the mixture of the reaction was heated to 100 Celsius for 30 min. When the temperature dropped to 37°C radio-HPLC was used to calculate and verify the radiolabeling yield [24–33].

Radiochemical analysis of [^{99m}Tc]tricarbonyl rolipram

Silica gel GF_{254} plates, (TLC-SG) sheets, were used to measure the radiochemical conversion percentage to [^{99m}Tc]-tricarbonyl rolipram complex. The sheets were marked using a non-pointed pencil at 2 cm from the bottom and 1 cm from the line up to 13 cm. Following Millipore filtration, a volume of 5 µL (1.60 MBq) of the [^{99m}Tc]-tricarbonyl rolipram of the reaction was detected utilizing a micropipette at the zero point, and allowed to evaporate. To create accurate separation, acetonitrile was used as the mobile phase. To evaluate the radioactivity, an SR.7 gamma

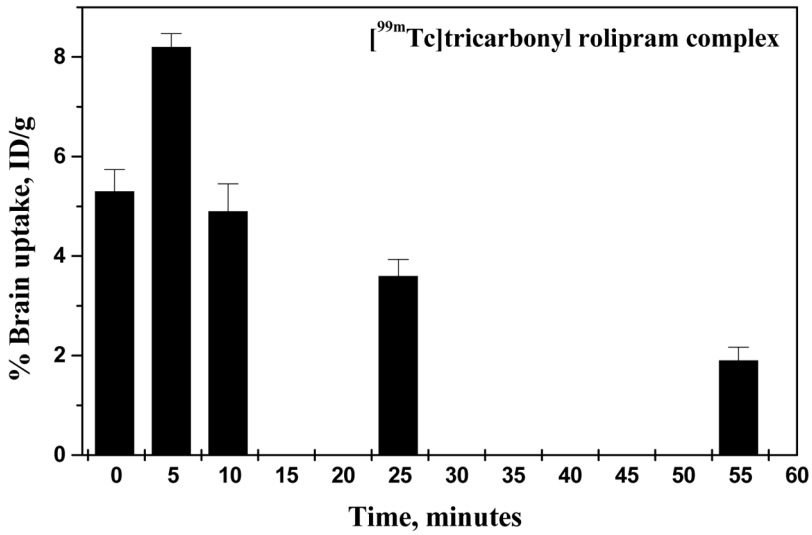

Fig. 4B. Brain uptake of [^{99m}Tc]tricarbonyl rolipram complex in normal male Swiss Albino mice as a function of time.

counter was used to count the dried and divided 1-cm TLC strips. Free [^{99m}Tc]-pertechnetate had a relative activity (R_f) of 0.3–0.4, whereas the [^{99m}Tc]-tricarbonyl rolipram complex had an R_f of 0.8–1.0 and the [^{99m}Tc]-tricarbonyl precursor had an R_f of 0.1 [34].

Physicochemical evaluation

Stability in rat serum media

In accordance with Motaleb, et al. and Sanad, et al. [24–27], the radiotracer [^{99m}Tc]tricarbonyl rolipram complex was analyzed in rat serum utilizing TLC or HPLC and then counted within a perfect scintillation counter to verify its stability [35].

Determination of the partition coefficient

The octanol/water partition coefficient ($P_{o/w}$) of the radiotracer [^{99m}Tc]tricarbonyl rolipram complex was determined at a pH value of 7.4 by measuring its distribution between octanol and phosphate buffered saline (PBS). A sample of 100 µL was added to an immiscible liquid containing PBS (900 µL, pH 7.4) and *n*-octanol (1 mL), then after 5 min of vigorous vortexing, the mixture was incubated for 30 min at room temperature. Centrifugation at 5000 rpm for 5 min

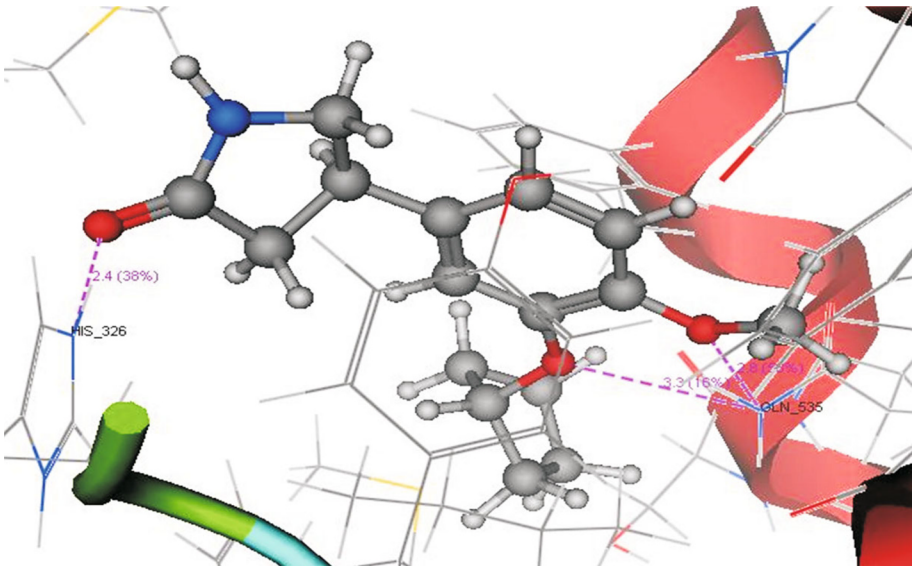

Fig. 5A. 3D Self-docking of rolipram showing interactions in PDE4 active site (PDB code 1TBB). It shows three hydrogen bonds (red-dotted line) with residues in the binding site.

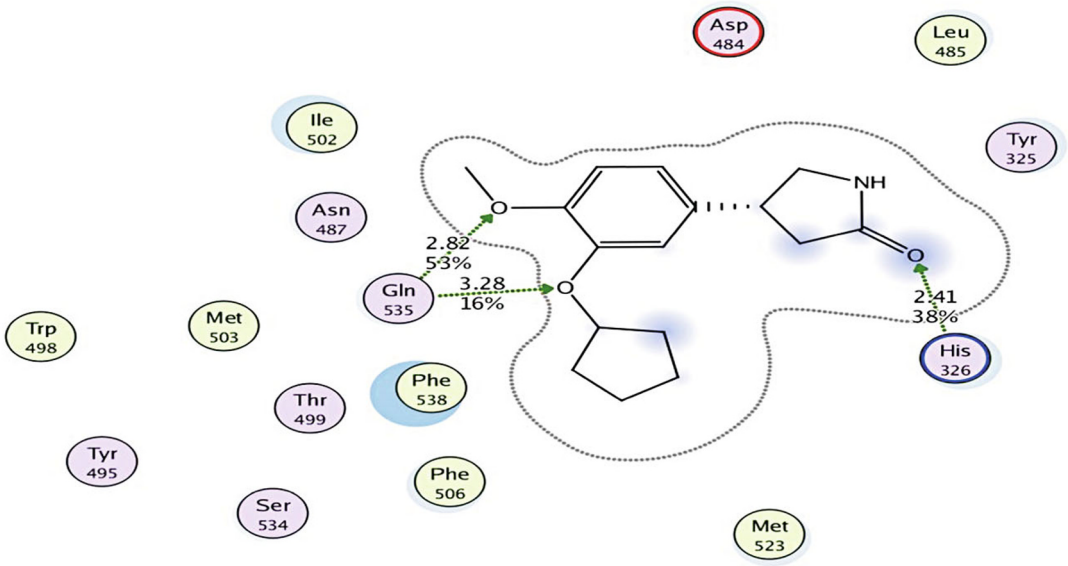

Fig. 5B. 2D Self-docking of rolipram showing interactions in the PDE4 active site (PDB code 1TBB). It shows three hydrogen bonds (green dotted arrows) with residues in the binding site.

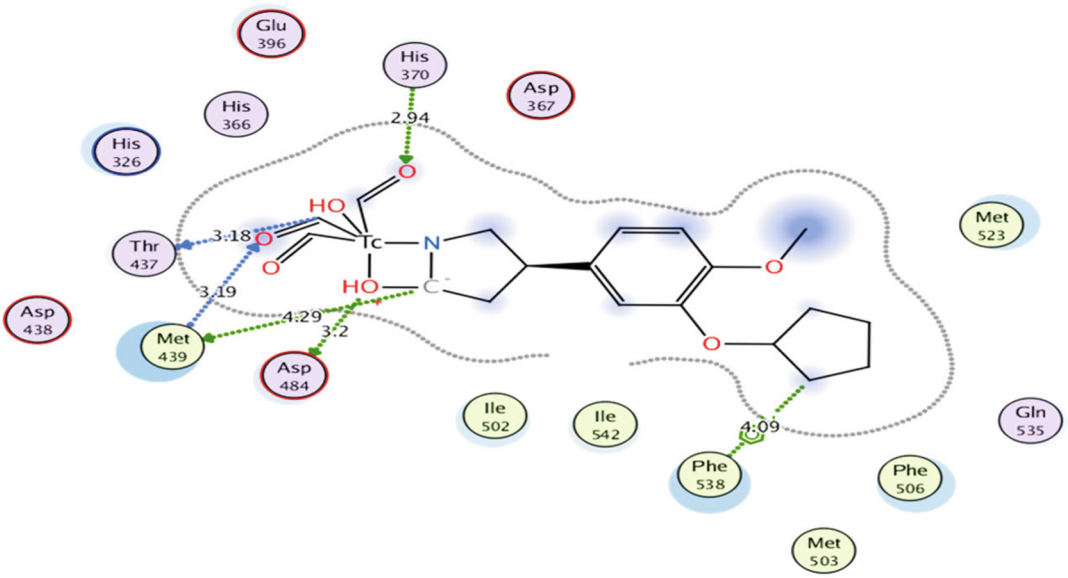

Fig. 5C. Top ranked 2D pose of [^{99m}Tc]tricarbonyl rolipram showing interactions in the PDE4 active site.

ensured complete separation of the organic and aqueous layers. An aliquot (100 µL) from each layer was measured using a γ-counter. The experiment was repeated five times. The partition coefficient value was expressed as log $P_{o/w}$ values.

Biodistribution and animal studies

Animal experiments were approved by the Ethics Committee of the Labeled Compounds Department. The mice were Swiss Albino mice (35–45 g). Five groups (5 mice for each group to give 25 mice in total) were intravenously injected with 100 µL (120–130 MBq) of sterile [^{99m}Tc]tricarbonyl rolipram complex via the tail vein and kept alive in metabolic cages for different intervals of time under normal conditions. These were used for quantitative determination of organ distribution (per time point) and sacrificed at various times post-injection (5 min, 10 min, 15 min, 30 min, and 1 h [23, 24]. All organs were separated and measured by comparison with a standard solution of the labeled substrate.

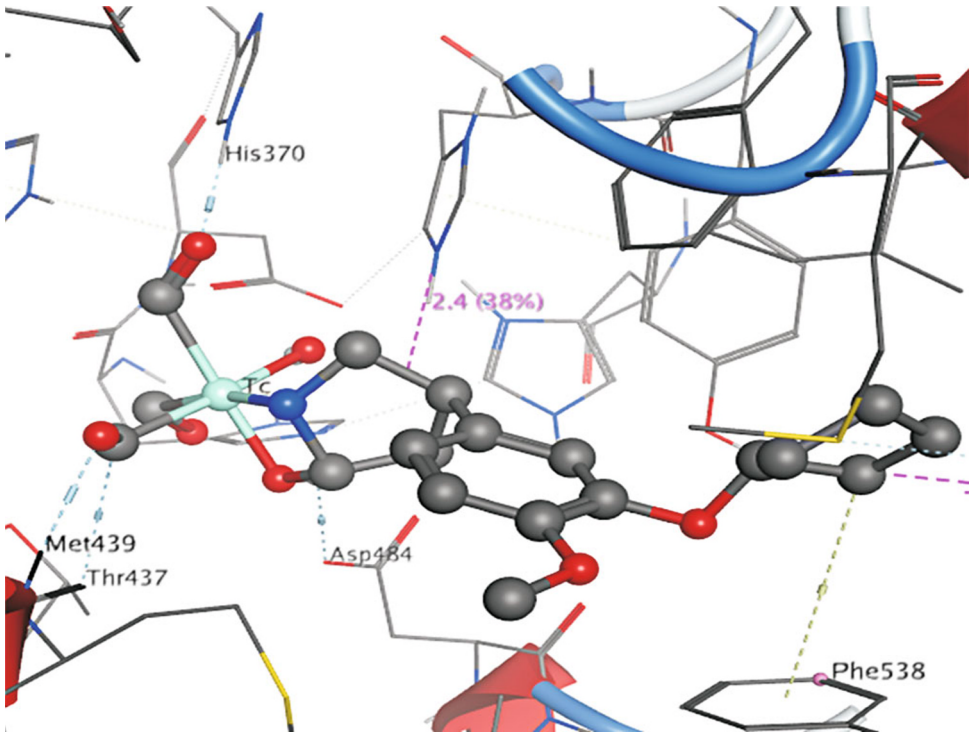

Fig. 5D. Top ranked 3D pose of [^{99m}Tc]tricarbonyl rolipram showing interactions in the PDE4 active site.

Fresh blood, bone, and muscle samples were also collected and measured. The mean percentage of the administered dose per gram was calculated. The ratios of blood, bone, and muscles were assumed to be 7, 10, and 40% of the total body weight respectively [36]. Corrections were made for background radiation and decay during the experiments. The data were estimated using a one-way ANOVA test. Results for P were reported and all the outcomes were given as mean ± SD. The level of significance was set at $P < 0.05$.

Blocking study of phosphodiesterase-4 inhibitor

Different amounts of unlabeled rolipram were used within the range 0–1000 µg. It was injected into the mice 10 min prior to administration of the radiotracer, and the percentage of brain uptake was estimated 10 min post-injection of heated radiotracer [^{99m}Tc]tricarbonyl rolipram complex ($n = 5$).

Molecular modeling

Docking simulations were performed using the structured preparation application in a Molecular Operating Environment (MOE), 2014.10 [18]. The x-ray crystallographic structure of Human Phosphodiesterase 4D (PDE4) in Com-

TABLE 1. Docking results (binding affinity, ligand amino acids interacted with binding site)

Compound	S-score	Amino acids involved in H-bonds	Amino acids involved in π-interaction
Rolipram	-11.3462	GLN 535 (2.82, 3.28 A°) HIS 326 (2.41 A°)	No
[^{99m}Tc]Tricarbonyl rolipram Proposed structure	-12.6890	THR437 (3.18 A°) MET439 (3.9, 4.29 A°) ASP484 (3.2 A°)	PHE 538

TABLE 2. The effect of rolipram amount on the radiolabeling yield of [^{99m}Tc]tricarbonyl rolipram

Rolipram (µg)	% [^{99m}Tc]tricarbonyl rolipram	% Free ^{99m}Tc	[^{99m}Tc(CO)$_3$(H$_2$O)$_3$]$^+$
precursor			
50	77.0 ± 0.18	12.5 ± 0.16	10.5 ± 0.19
75	82.0 ± 0.13	5.0 ± 0.15	13.0 ± 0.76
100	97.0 ± 0.19	1.6 ± 0.16	1.4 ± 0.17
150	97.2 ± 0.39	1.3 ± 0.33	1.5 ± 0.76
200	96.0 ± 0.18	1.8 ± 0.19	2.2 ± 0.21
250	95.5 ± 1.10	2.1± 0.19	2.4 ± 0.11
300	95.0 ± 0.15	2.6 ± 0.19	2.4 ± 0.12

Values represent the mean ± SEM, $n = 3$

plex with Rolipram (PDB code: 1TBB) was retrieved from the Protein Data Bank of the Research Collaboration for Structural Bioinformatics (RCSB) website (www. rcsb.org] [18 – 20].

RESULTS AND DISCUSSION

Thin-layer chromatography analysis

The results of thin-layer chromatography revealed that The *Rf* values for the [^{99m}Tc] tricarbonyl rolipram complex, free pertechnetate, and [^{99m}Tc] tricarbonyl core were 0.9–1.0, 0.3–0.4, and 0.1 respectively. The radiochemical yield of the [^{99m}Tc]tricarbonyl rolipram complex right after the synthesis was over 98%, which could be estimated by subtracting the relative percentage concentration of the remaining species from 100%.

High-performance liquid chromatography analysis

At a flow frequency of 0.6 mL/min, with Rt = 11.30 min for free [^{99m}Tc] pertechnetate and Rt = 4.4 min for the [^{99m}Tc] tricarbonyl core (see Fig. 3A) a radiochemical conversion efficiency of 97.0% was achieved; moreover, the HPLC of the [^{99m}Tc] tricarbonyl rolipram complex was also determined to be 98%. Free [^{99m}Tc]tricarbonyl core Rt was 4.9 min, whereas the rolipram complex Rt was 9.0 min (see Fig. 3B).

Reaction optimization

The radiochemical yield of [^{99m}Tc]tricarbonyl rolipram complex was increased to 97% by optimizing many factors (pH, substrate quantity, and temperature). When the rolipram amount was increased to 100 μg (7.5 MBq), the radiochemical conversion to the complex [^{99m}Tc]tricarbonyl rolipram reached a maximum of 97.0% (Table 1). All other reaction parameters were held constant. Additionally, the optimality of the reaction mixture was demonstrated at a pH of 9.0, which may be a reflection of the stability of the complex, [^{99m}Tc]tricarbonyl rolipram. It was also determined that 30 min was the optimal period for the reaction, yielding a radiochemical conversion of 97.0%. The compound has been shown to be stable in rat serum. [^{99m}Tc]Tricarbonyl rolipram complex was noted to be stable up to 24 h to give 95%; after that, the purity reduced to 80.0% at 48 h.

Biodistribution studies

By tracing the radiotracer [^{99m}Tc] tricarbonyl rolipram complex it was distributed in a variety of tissues and bodily fluids, as represented in Table 2. All radioactivity measurements are represented as the mean standard deviation of the injected activity per gram of tissue (%ID/g). The distribution of the radiotracer revealed that the concentration in the liver reached 22.30% at 30 min p.i., and then declined to 12.29% 1 h later. Renal absorption reached 19.34% at 30 min p.i. and declined to 6.77% p.i. at 1 h, which led to the conclusion that the hepatobiliary and urinary systems are responsible for washing away the radiotracer [^{99m}Tc]tricarbonyl rolipram complex [16]. Results also revealed a low stomach concentration at all times, indicating that the radiotracer [^{99m}Tc]tricarbonyl rolipram complex is stable in vivo. The rapid distribution of the radiotracer [^{99m}Tc]tricarboxylic rolipram complex in most organs was evident at 5 min p.i. Most of the complex was absorbed by the brain at 10 min p.i., giving 8.20%. This difference in the uptake of the radiotracer (p.i.)

TABLE 3. Biodistribution of [^{99m}Tc]tricarbonyl rolipram in normal mice at different times

Organs and body fluids	% I.D./g at different times post-injection				
	5 min	10 min	15 min	30 min	60 min
Blood	5.6 ± 0.44	3.8 ± 0.12	2.88 ± 0.32	2.20 ± 0.01	1.3 ± 0.12
Bone	1.4 ± 0.15	1.3 ± 0.12	1.2 ± 0.17	1.10 ± 0.12	0.9 ± 0.02
Muscle	3.1 ± 0.25	2.4 ± 0.27	2.1 ± 0.29	1.60 ± 0.20	1.11 ± 0.13
Brain	5.3 ± 0.44	8.2 ± 0.21	4.9 ± 0.27	3.60 ± 0.12	1.90 ± 0.15
Lungs	1.13 ± 0.12	1.11 ± 0.22	1.0 ± 0.09	0.09 ± 0.06	0.08 ± 0.07
Heart	1.4 ± 0.20	1.3 ± 0.11	1.22 ± 0.06	1.12 ± 0.13	0.98 ± 0.08
Liver	5.33 ± 0.15	8.11 ± 0.23	14.20±0.89	22.30 ± 0.55	12.29 ± 0.33
Kidneys	4.9 ± 0.32	8.77 ± 0.54	11.76 ± 0.85	19.34 ± 0.87	6.77 ± 0.33
Spleen	1.32 ± 0.20	1.22 ± 0.44	1.12 ± 0.65	1.00 ± 0.07	0.99 ± 0.08
Intestine	1.9 ± 0.66	2.8 ± 0.84	3.47 ± 0.22	5.66 ± 0.66	3.22 ± 0.21
Stomach	1.3 ± 0.32	1.2 ± 0.11	1.11 ± 0.08	1.00±0.07	0.99±0.09
Brain/Blood	0.95	2.16	1.70	1.64	1.46

Mean±SEM (mean of five experiments)

in brain could be attributed to the difference in accumulation selectively to phosphodiesterase-4 inhibitor (PDE4) receptors. By comparing this brain uptake of [^{99m}Tc] tricarbonyl rolipram complex (8.20% ID/g at 10 min p.i.), % ID/g organ ± S. D, amount with part of the available labeled compounds indicated that this uptake is considered more than them. These results are confirmed by rolipram complex inhibition (see Fig. 4A). In addition, the brain-to-blood ratios of [^{125}I]iodorolipram were 0.95, 2.16, 1.70, 1.64 and 1.46 at 5,10, 15, 30, and 60 min respectively (see Fig. 4B). The uptake of the radiotracer [^{99m}Tc]tricarbonyl rolipram complex is higher than the reported corresponding values for other agents such as [^{99m}Tc]HMPAO, which showed 3.50% ID/g at 30 min p.i. in rats, [^{99m}Tc]ECD complex, which showed 4.7% ID/g at 24 h p.i. in monkey, and [^{125}I]iodorolipram, which showed 7.60% ID/g at 10 min p.i. in mice. Our results indicate that iodorolipram has superior % ID/g ± S. D. value than commercially available complexes ([^{99m}Tc]HMPAO and [^{99m}Tc]ECD) [13, 14].

Lipophilicity

The lipophilicity of the radiotracer [^{99m}Tc]tricarbonyl rolipram complex was determined by measuring the partition coefficient between octanol and phosphate buffer 0.1 M, pH 7.4. A log *p* value of 2.66 ± 0.23 indicates the ability of the radiotracer [^{99m}Tc]tricarbonyl rolipram complex to cross the blood brain barrier [30 – 40].

Blocking study of phosphodiesterase-4 inhibitor

Pre-dosing albino mice with unlabeled rolipram, using different amounts of rolipram (250–1000 μg), 10 min before the injection of the radiotracer [^{99m}Tc]tricarbonyl rolipram complex reduced the brain uptake from 8.2 to 1.3 %ID/g organ at 10 min p.i. This result suggested that the radiotracer [^{99m}Tc]tricarbonyl rolipram complex binds selectively to phosphodiesterase-4 inhibitor (PDE4) receptors in the brain and that the uptake was specific. As a result of this study, the radiotracer [^{99m}Tc]tricarbonyl rolipram complex can be used successfully in imaging of the PDE4 receptor (see Fig. 4A). These results are in agreement with previous reports [31].

Molecular modeling studies

The main objective of performing molecular modeling studies is to compare between the binding modes of rolipram (ROL) co-crystalized ligand of PDE4 (PDB code: 1TBB) and [^{99m}Tc] tricarbonyl rolipram. As shown in Table 1, rolipram had an S-score of -11.3462 and exhibited three hydrogen bonds: two with GLN 535 of distances (2.82, 3.28 A°) and the last one with HIS 326 of distance (2.41 A°) (Figs. $5_{A\text{-}B}$,). Moreover, docking results of the proposed [^{99m}Tc] tricarbonyl rolipram structure showed that it can interact with 1TBB, as shown in Table 1. The proposed [^{99m}Tc]Tricarbonyl rolipram structure has an S-score of -12.6890 and exhibited four hydrogen bonds: one with THR 437 with a distance of (3.18 A°); two with a MET 439 with a distance of (3.9 and 4.29 A°); and one with an ASP 484 with a distance of (3.2 A°), in addition to a π-interaction with PHE 538 (Figs. $5_{C\text{-}D}$,). Conclusively labeling rolipram with [^{99m}Tc] tricarbonyl did not disturb its binding to phosphodiesterase-4.

CONCLUSION

An optimized protocol for the synthesis of the radiotracer [^{99m}Tc]tricarbonyl rolipram complex in a high yield has been elaborated. Bio-distribution studies indicated that the radiotracer [^{99m}Tc]tricarbonyl rolipram complex has a high brain uptake of 8.2% ID/g at 10 min. This ID/g value is provisionally improved over agents such as [^{99m}Tc]ECD, [^{99m}Tc]HMPAO, and [^{125}I]iodorolipram radiotracers. Therefore, the radiotracer [^{99m}Tc]tricarbonyl rolipram could be considered a new potential selective radiotracer for brain imaging.

Authors' Contributions

M. H. Sanad: development of the research idea, conceptualization, methodology, biodistribution, validation, investigation, labeling, and writing the original draft; H. M. Eyssa: resources and methodology; S. M. Abd-Elhaliem: participated in developing the research idea, resources, labeling, and biodistribution; A. B. Farag: formal analysis, visualization, and molecular modeling studies; S. A. Bassem: biodistribution, writing (review and editing), and supervision.

Ethics Approval

All applicable national, international, and institutional guidelines for the care and use of animals were followed. Animal studies were approved by the Labeled Compounds Department, Egyptian Atomic Energy Authority. This article does not contain any human studies performed by any of the authors.

Disclosures Statement

Data Availability Statement

All research data were compiled at the Egyptian Atomic Energy Authority.

Funding

No funding has been provided for the publication or carrying out of the current academic research.

Conflicts of interest statement

The authors declare that there are no conflicts of interest.

REFERENCES

1. A. T. Eggebrecht, B. R. White, S. L. Ferradal, et al., *Neuroimaging*, **61**(4), 1120–1128 (2012).

2. S. D. Silberstein, *Neurology*, **55**(6), 754–762 (2000).
3. J. J. Sung, E. J. Kuipers, H. B. El-Serag, *Aliment. Pharmacol. Ther.*, **29**(9), 938 – 946 (2009).
4. A. Vcev, D. Stimac, A. Vceva, et al., *Helicobacter*, **4**(1), 54 – 57 (1999).
5. D. R. Scott, G. Sachs, E. A. Marcus, *F1000Res.*, **19**(5), 1747 (2016).
6. M. H. Sanad, H. A. Shweeta, *J. Mol. Imag. Dynamic*, **5**, 1 – 3 (2015).
7. Z. Mengzhu, L. Shanshan, G. Suyu, et al., *Oncotarget*, **8**(24), 39143 – 39153 (2017).
8. J. R. Bruno, Nicolaus, *Drug Dev. Res*., **2**(5), 463 – 474 (1982).
9. H. B. Hupf, J. S. Eldridge, J. Beaver, *Appl .Radiat. Isot.*, **19**(4), 345–351(1968).
10. D. Kwon, J. B. Chae, C. W. Park, et al., *Arzneimittelforschung*, **51**(3), 204 – 213 (2001).
11. M. H. Sanad, A. A. Ibrahim, *Radiochim. Acta*, **106**(10), 843 – 850 (2018).
12. M. A. Motaleb, M. H. Sanad, A. A. Selim, et al., *Int. J. Radiat. Biol.*, **94**(6), 590 – 596 (2018)
13. R. D. Neirinckx, L. R. Canning, I. M. Piper, et al., *J. Nucl. Med*., **28**, 191–202 (1987).
14. R. C. Walovitch, T. C. Hill, S. T. Garrity, et al., *J. Nucl. Med*., **30**, 1892–1901(1989).
15. S. M. H. Sanad, D. H. Hanna, A. E. M. Mekky, *J. Mol. Struct.*, **1188**, 214 – 226 (2019).
16. M. H. Sanad, A. A. Ibrahim, H. M. Talaat, *J. Radioanal. Nucl. Chem*., **315**(1), 57 – 63 (2018).
17. R. Alberto, R. Schibli, A. P. Schubiger, *J. Am. Chem. Soc*., **121**(25), 6076 – 6077 (1999).
18. Molecular Operating Environment (MOE). 2008.10., Chemical Computing Group Inc., 1010 Sherbooke St. West, Suite #910, Montreal, QC, Canada, H3A, 2R7 (2008).
19. M. Na?m, S. Bhat, K. N. Rankin, et al., *J. Chem. Infor. Mode*, **47**(1), 122 – 133 (2007).
20. P. Labute, *Proteins*, **75**(1), 187 – 205 (2009).
21. M. A. Motaleb, A. A. Selim., M. El-Tawoosy, et al., *Radioanal. Nucl. Chem.*, **314**, 1517 – 1522 (2017).
22. P. Unak, F. Y. Lambrecht, F. Z. Biber, et al., *J. Radioanalyt. & Nucl. Chem.*, **261**(3), 587 – 591 (2004).
23. M. H. Sanad, H. M. Talaat, *Radiochemistry*, **59**, 396 – 401(2017).
24. S. F. A. Rizvi, H. Zhang, S. Mehamood, M. H. Sanad, *Transl. Oncol*., **13**(12), 100854 (2020).
25. K. Jeffrey, L. Malgorzata, T. T. Andrew, et al., *Eur. J. Inorg. Chem*., **27**, 4334 – 4341 (2012).
26. L. Malgorzata, K. Jeffrey, G. Luigi, et al., *J. Nucl. Med.*, **53**(8), 1277 – 1283 (2012).
27. B. A. Rhodes, *Semin. Nucl. Med*., **4**, 281 – 293 (1974).
28. W. Duangporn, *World J. Gastroenterol.*, **20**(21), 6420 – 6424 (2014).
29. M. A. Peppercorn, P. Goldman, *Therapeutics*, **181**(3), 555 – 562 (1972).
30. J. B. Wiggins, R. B. Rajapakse, *Drug. Metab. Toxicol.*, **5**(10), 1279 – 84 (2009).
31. M. B. Zhang, J. Y. Han, Z. Y. Huang, *Chin. J. Pharm. Anal.*, **21**(4), 253 – 254 (2001).
32. B. A. Rhodes, *Semin. Nucl. Med.*, **4**(3), 281 – 293 (1974).
33. M. H. Sanad, E. Borai, *J. Anal. Sci. Technol*., **5**, 32 (2014).
34. P. Unak, F. Y. Lambrecht, F. Z. Biber, et al., *J. Radioanal. Nucl. Chem*., **261**(3), 587– 591 (2004).
35. M. H. Sanad, M. A. Abelrahman, F. M. A. Marzook, *Radiochim. Acta*, **104**(5), 345 – 353 (2016).
36. A. K. Mohammad, H. Abolfazl, *Iran J. Org. Chem*., **4**, 268 – 270 (2009).
37. H. Abolfazl, A. K. Mohammad, H. Masoumeh, et al., *Monthly Chem*., **143**, 619 – 623 (2012).
38. M. H. Sanad, E. A. Marzook, S. B. Challan, *Radiochim. Acta*, **106**(4), 329 – 336 (2018).
39. R. Pasqualini, V. Comazzi, E. Bellande, et al., *Appl. Radiat. Isotopes*, **43**(11), 1329 – 1333 (1992).
40. M. E. Moustapha, M. A. Motaleb, M. H. Sanad, *J. Radioanal. Nucl. Chem*., **309**(2), 511 – 516 (2016).